ESTIMATING A SHEAR MODULUS OF A TRANSVERSELY ISOTROPIC FORMATION

by

K. J. Ellefsen, C. H. Cheng, and M. N. Toksöz

Earth Resources Laboratory
Department of Earth, Atmospheric, and Planetary Sciences
Massachusetts Institute of Technology
Cambridge, MA 02139

ABSTRACT

A method to estimate c_{66}, which is a shear modulus of a transversely isotropic formation (with its symmetry axis parallel to the borehole), is developed and tested. The inversion for c_{66} is based upon a cost function which has three terms: a measure of the misfit between the observed and predicted wavenumbers, a measure of the misfit between the current estimate for c_{66} and the initial guess of its value, and penalty functions which constrain the estimate for c_{66} to physically acceptable values. The inversion is applied to synthetic data for fast and slow formations, and the estimates for c_{66} are within 5% of their correct values and are well resolved. The inversion is applied to field data from a formation which consists mostly of siltstone. All estimates for c_{66} are significantly higher than for c_{44}, and the S-wave anisotropy generally ranges from 19 to 24%.

INTRODUCTION

In sedimentary basins, transverse isotropy with a vertical symmetry axis is the largest component of anisotropy. Field measurements indicate that the velocity of the horizontally polarized S-wave in transversely isotropic formations can be 10 to 30% higher in the horizontal direction than in the vertical direction (White et al., 1983; Winterstein, 1986). In contrast, azimuthal variations in S-wave velocity generally range from 3 to 5%, and those in P-wave velocity are even less (S. Crampin, 1988, oral communication; D. Corrigan, 1989, oral communication; D. F. Winterstein, 1989, oral communication).

An important question is: can acoustic logging be used to estimate the elastic properties of these transversely isotropic formations? White and Tongtaow (1981) and Chan and Tsang (1983) found that the velocities of the refracted P and S waves are $\sqrt{c_{33}/\rho}$ and $\sqrt{c_{44}/\rho}$, respectively. Consequently, if the formation density is known,

then the refracted waves can be used to estimate c_{33} and c_{44}. White and Tongtaow also developed a formula which relates the velocity of the tube wave at the zero frequency limit to c_{66}, but when data at low frequencies (i.e., less than about 200 Hz) are unavailable this formula cannot be used.

In this paper, a method is developed to estimate c_{66} of a transversely isotropic formation (with its symmetry axis parallel to the borehole) using the wavenumbers from the tube wave. These wavenumbers are shown to be moderately sensitive to c_{66} over a wide range of frequencies for most transversely isotropic formations, and this sensitivity is the basis of the inversion. A robust procedure for the inversion is developed, and its performance is evaluated using synthetic data from fast and slow formations. Field data are used to estimate c_{66} in a siltstone.

METHOD

Formulation

The inversion is based upon a mathematical model of the borehole environment (Figure 1). The fluid is perfectly elastic, its incompressibility is λ_1, and its density is ρ_1. The borehole wall is perfectly round, and its radius is R. The formation is perfectly elastic and homogeneous. Because the formation is transversely isotropic with its symmetry axis parallel to the borehole, its elastic properties are specified by only five moduli: c_{11}, c_{13}, c_{33}, c_{44}, and c_{66} which are written in abbreviated subscript notation. The density of the formation is ρ_2.

The procedure by which c_{66} is estimated is based upon a cost function that has three terms. The first term contributes information about the data, the second about the original estimate of c_{66}, and the third about the physical constraints on c_{66}. These three terms will now be developed.

The first term in the cost function requires that the wavenumbers predicted by the forward model closely match the observed wavenumbers. Array processing of seismograms from multi-receiver tools is used to estimate the wavenumber, amplitude, attenuation, and phase of each guided wave at all frequencies (Parks et al., 1983; McClellan, 1986; Ellefsen et al., 1989). The estimated wavenumbers are arranged in a vector denoted $\mathbf{d}_{obs}$. Because the amplitude estimates indicate the accuracy of the wavenumber estimates, they are used to develop the data covariance matrix, $\mathbf{C}_D$. The matrix is diagonal because all wavenumber estimates are assumed to be independent. Wavenumbers for the current forward model are calculated with the dispersion equation. These predicted wavenumbers are arranged in a vector denoted $\mathbf{g}(m)$, where m represents the current estimate of c_{66}. In terms of probability theory, the relationship between the observed and predicted wavenumbers may be expressed by the generalized

Gaussian density function:

$$f_p(m) = K_1 \exp\left[-\frac{1}{p}(|\mathbf{d}_{obs} - \mathbf{g}(m)|^{p/2})^T \mathbf{C}_D^{-1}(|\mathbf{d}_{obs} - \mathbf{g}(m)|^{p/2})\right] \quad (1)$$

(Tarantola, 1987, p. 26-28) where K_1 is a normalizing constant. The important property of $f_p(m)$ is that when p is close to 1 $f_p(m)$ decreases slowly away from its maximum value at $\mathbf{d}_{obs} = \mathbf{g}(m)$. Hence, a few observed wavenumbers can deviate significantly from their correct value without seriously affecting the solution. This property makes the inversion robust. Maximizing the probability density function is equivalent to minimizing the negative of its exponent,

$$\frac{1}{p}(|\mathbf{d}_{obs} - \mathbf{g}(m)|^{p/2})^T \mathbf{C}_D^{-1}(|\mathbf{d}_{obs} - \mathbf{g}(m)|^{p/2}) \quad , \quad (2)$$

which will be the first term in the cost function.

The second term in the cost function requires that c_{66}, which is estimated during the inversion, be close to the initial estimate of its value. A cross-plot of c_{44} and c_{66}, which is based upon laboratory and field measurements of transversely isotropic rocks, indicates that when c_{44} is known the range of acceptable values for c_{66} is well defined (Figure 2). Consequently the cross-plot is used to estimate the most-likely value of c_{66} (which is used for the initial value of c_{66} in the inversion, m_o) and the standard deviation of c_{66} (σ_m). The relationship between m_o and the model parameter predicted by the inversion, m, may be expressed by the normal density function:

$$\rho_M(m) = K_2 \exp\left[-\frac{1}{2}(m - m_o)(\sigma_M^2)^{-1}(m - m_o)\right] \quad (3)$$

where K_2 is a normalizing constant. Maximizing this density function is equivalent to minimizing the negative of its exponent,

$$\frac{1}{2}(m - m_o)(\sigma_M^2)^{-1}(m - m_o) \quad , \quad (4)$$

which will be the second term in the cost function.

The third term in the cost function requires that the elastic moduli be physically possible. The elastic strain energy density, $\frac{1}{2}e_I c_{IJ} e_J$, is always positive for any nonzero strain, e_I. Hence, the matrix of elastic moduli, c_{IJ}, must be positive definite. For a transversely isotropic medium, this requirement is met when

$$c_{11} - |c_{11} - 2c_{66}| > 0 \quad , \quad (5)$$

$$(c_{11} - c_{66})c_{33} - c_{13}^2 > 0 \quad , \quad (6)$$

and

$$c_{44} > 0 \quad (7)$$

(Auld, 1973, p. 147-149). Only the first two equations are needed for the inversion. They are written symbolically as $h_i(m) > 0$ (where i is an equation index) and are used to develop penalty functions,

$$\psi_i = \frac{\alpha_i}{h_i(m)} \quad , \tag{8}$$

where α_i is a small, positive constant (Bard, 1974, p. 141-145). The penalty functions are written in vector form as $\mathbf{\Psi}$, and the inner product,

$$\mathbf{\Psi}^T \mathbf{\Psi} \quad , \tag{9}$$

is the third term in the cost function. For almost values of c_{66}, this term is negligibly small. As c_{66} approaches the region in which the Eqs (5) and (6) are not satisfied, this term becomes very large and significantly increases the cost function.

The cost function used by the inversion combines the expressions in (2), (4), and (9):

$$\begin{aligned} \Phi(m) \quad = \quad & \frac{1}{p}(|\mathbf{d}_{obs} - \mathbf{g}(m)|^{p/2})^T \mathbf{C}_D^{-1}(|\mathbf{d}_{obs} - \mathbf{g}(m)|^{p/2}) + \\ & \frac{1}{2}(m - m_o)(\sigma_M^2)^{-1}(m - m_o) + \mathbf{\Psi}^T \mathbf{\Psi} \quad . \end{aligned} \tag{10}$$

This cost function is minimized with respect to m to find the best choice for c_{66}.

Optimization Technique

An approximate technique is used to minimize the cost function (Eq. 10). The differences between the observed and predicted wavenumbers are the residuals: $r_i = (d_i)_{obs} - g_i(m)$. A diagonal weighting matrix, $\mathbf{W}$, is defined from these residuals:

$$W_{ii} = \begin{cases} (\epsilon/|r_i|)^{2-p} & \text{if } |r_i| > \epsilon \\ 1 & \text{if } |r_i| \leq \epsilon \end{cases} \tag{11}$$

where ϵ is a small positive constant and $1 \leq p \leq 2$ (Scales and Gersztenkorn, 1988). The cost function is now rewritten as

$$\begin{aligned} \Phi(m) \quad = \quad & \frac{1}{p}(|\mathbf{d}_{obs} - \mathbf{g}(m)|^{p/2})^T \mathbf{W}^{1/2} \mathbf{C}_D^{-1} \mathbf{W}^{1/2}(|\mathbf{d}_{obs} - \mathbf{g}(m)|^{p/2}) + \\ & \frac{1}{2}(m - m_o)(\sigma_M^2)^{-1}(m - m_o) + \mathbf{\Psi}^T \mathbf{\Psi} \quad . \end{aligned} \tag{12}$$

This equation shows that $\mathbf{W}$ prevents large residuals from significantly increasing the cost function and adversely affecting the estimate for m. The advantage of this formulation is that standard least-squares algorithms can be used to perform the optimization.

The cost function is minimized using a Levenburg-Marquardt algorithm which has been developed for nonlinear, least-squares problems (Moré, 1978; Moré et al., 1980). The Jacobian matrix, which is required for this algorithm, is calculated using a perturbation method. When the inversion finds an acceptable solution, the costs associated with the constraints are virtually zero. If the product $p\mathbf{W}^{-1/2}\mathbf{C}_D\mathbf{W}^{-1/2}$ is interpreted as a data covariance matrix which is continually being adjusted, then the optimization is similar to the maximum likelihood inversion (Aki and Richards, 1980, p. 690-692).

Resolution of the Estimate

To evaluate the estimate for c_{66}, its final standard deviation is compared to its initial standard deviation. If the deviation has been significantly reduced, then c_{66} is well resolved. The final standard deviation is the square root of the final model variance,

$$\sigma_{M'}^2 \approx \left[\mathbf{G}^T\mathbf{C}_D^{-1}\mathbf{G} + (\sigma_M^2)^{-1}\right]^{-1} \qquad \text{for } p = 2, \tag{13}$$

(Tarantola, 1987, p. 196-198) where $G_{ij} = \partial g_i/\partial m_j$. This formula is only approximate because the problem is nonlinear. No formula for $\sigma_{M'}^2$ exists when $1 \leq p < 2$, but this relation may still be used for a crude estimate of $\sigma_{M'}^2$.

RESULTS AND DISCUSSION

Sensitivity of the Data to the Elastic Moduli

To properly perform an inversion, the sensitivity of the wavenumbers to the different elastic moduli must be determined. This sensitivity can be expressed quantitatively with the normalized partial derivative of the wavenumber with respect to an elastic modulus of the formation, c_{IJ}^{TI}:

$$\frac{c_{IJ}^{TI}}{k_z}\frac{\partial k_z}{\partial c_{IJ}^{TI}} \quad .$$

Similarly, the sensitivity associated with the incompressibility of the fluid is

$$\frac{\lambda_1}{k_z}\frac{\partial k_z}{\partial \lambda_1} \quad .$$

The sensitivities were calculated for the normal modes in fast, slow, and very slow formations (Tables 1, 2, and 3) using a perturbation method. Ellefsen et al. (1988) examined the sensitivities of all normal modes to demonstrate that the best data for estimating c_{66} come from the low frequency portion of the tube wave. The sensitivities for this part of the tube wave will be discussed here in the context of the inversion.

In many respects, the sensitivities for the fast and slow formations (Figures 3, 4, 5, and 6) are similar. The wavenumbers are more sensitive to λ_1 than they are to c_{66}, and therefore λ_1 must be accurately known before c_{66} can be estimated. The wavenumbers are insensitive to c_{11} and c_{13}, and consequently using any reasonable value for these unknown moduli will not adversely affect the inversion. Because the data are insensitive to c_{33} and only moderately sensitive to c_{44} near 5 kHz, inaccurate values for these moduli, which are determined from the refracted waves and the flexural wave, will not affect the estimate of c_{66} much.

The sensitivities for the non-leaky tube wave in the very slow formation (Figures 7 and 8) are very different from those in the previous two examples. In general, the wavenumbers are very sensitive to c_{44}, moderately sensitive to c_{11}, c_{13}, c_{33}, and c_{66}, and insensitive to λ_1. Because the sensitivities for c_{11} and c_{13} are roughly equal to that for c_{66} and because c_{11} and c_{13} are unknown, c_{66} cannot be estimated.

An important issue is knowing when c_{66} can be reliably estimated. To this end, examine the sensitivities for the fast, slow, and very slow formations (Figures 3, 5, 7, and Figures 4, 6, 8 in these orders). The sensitivities for λ_1 generally decrease, and the sensitivities for c_{11}, c_{13}, c_{33}, and c_{44} increase. The sensitivity of c_{66} does not change as much between the three formations as the sensitivities of the other moduli do. To accurately estimate c_{66}, the sensitivities for c_{11} and c_{13}, which are not precisely known, must be small compared to the sensitivity of c_{66}. As a rule of thumb, this situation occurs when the velocity of the vertically propagating S wave is greater than or approximately equal to the acoustic velocity of the fluid.

Testing the Inversion with Synthetic Data

The inversion for c_{66} was tested first with synthetic data calculated for the model with the fast formation (Table 1). Synthetic seismograms (Figure 9) were processed to extract the wavenumber and amplitude estimates for the tube wave (Figures 10 and 11). Then values for the elastic moduli of the formation were selected. Values for c_{33} and c_{44} were determined from the refracted P and S waves, respectively. (Although the refracted P wave is not evident in Figure 9, it can be seen if the amplitudes are increased.) Values for c_{11} and c_{13} were determined from cross-plots of the elastic moduli of transversely isotropic rocks (Figures 12 and 13). (In Figure 13, c_{13} depends strongly on the linear combination, $c_{33} - 2c_{44}$. To understand this result, assume for a moment that the rock is isotropic. The elastic moduli in terms of the Lamé parameters are $c_{11} = c_{33} = \lambda + 2\mu$, $c_{13} = \lambda$, and $c_{44} = c_{66} = \mu$. When a rock is only slightly anisotropic, $c_{33} - 2c_{44}$ is close to c_{13}.) The starting value for c_{66} and its standard deviation, 0.35×10^{10} Pa, were estimated from the cross-plot with c_{44} (Figure 2). Because the formation density, fluid density, and borehole radius are normally measured in field situations, they were set to their correct values. Because λ_1

can be estimated from the first mode of the leaky P-wave (using a technique which will be demonstrated later), λ_1 was set to its correct value. All of the model parameters used in the inversion are summarized in Table 1. Only data below 4 kHz were used, and p was chosen to be 1.8 because the data contain little noise. For this inversion, the cost function is dominated by the term associated with the data (Figure 14) indicating that the estimated value for c_{66} depends almost entirely upon the data and not upon the initial estimate of its value or the constraints. The cost surface (Figure 15) has no local minima over the range of values which c_{66} might have, and hence convergence to the global minimum is guaranteed. The estimated value for c_{66} is 0.92×10^{10} Pa which differs from the correct value by only 0.04×10^{10} Pa. c_{66} is well resolved: the final standard deviation is 0.03×10^{10} Pa, which is much smaller than the initial standard deviation (0.35×10^{10} Pa).

Then the inversion was tested with synthetic data calculated for the model with the slow formation (Table 2). The generation of synthetic seismograms, array processing, and inversion for the slow formation followed the same procedures used in the fast formation. The model parameters for the inversion are listed in Table 2. The standard deviation was estimated from Figure 2 to be 0.35×10^{10} Pa, and p was chosen to be 1.8. Because the cost function is dominated by the term associated with the data (Figure 16), the estimated value for c_{66} depends upon the data and not on the initial estimate or the constraints. Because the cost surface has no local minima (Figure 17), convergence to a global minimum is guaranteed. The estimated value for c_{66} is 1.11×10^{10} Pa which differs from the correct value by 0.06×10^{10} Pa. Again c_{66} is well resolved because the standard deviation was reduced from 0.35×10^{10} Pa to 0.02×10^{10} Pa.

For both inversions, the exact value of c_{66} was not estimated. This inaccuracy may be due to errors introduced into the inversion by the approximate values which were chosen for c_{11}, c_{13}, c_{33}, and c_{44} (Tables 1 and 2). Nonetheless, each estimated value for c_{66} is within 5% of its correct value.

Field Data

The acoustic logging data were collected by a tool having 12 receivers and 2 sources. The other measurements which were made in this well include the shear, caliper, gamma ray, and density logs. In several zones, cores were cut, and the permeabilities of the rock were measured.

To determine the incompressibility of the fluid, seismograms from a zone with a very slow formation (Figure 18) were processed to calculate the phase velocities of the leaky P wave (Figure 19). These phase velocities asymptotically approach the acoustic velocity of the fluid. Judging from this dispersion curve, the acoustic velocity of the fluid is approximately 1.52 km/s. Because the fluid density is 1.10×10^3 kg/m^3, the

incompressibility of the fluid is approximately 0.255×10^{10} Pa.

Because the logging tool affects the tube wave, the inversion must be modified. The most direct method of accounting for its effects is to develop a new mathematical model and then derive a new dispersion equation. The tool near the receivers consists of a steel cable, 12 transducers mounted on the cable, a layer of oil which surrounds the cable and the transducers, and a rubber housing. Incorporating these features in the mathematical model would be difficult, and the resulting dispersion equation would be very complicated. An alternative method of accounting for the tool is based on the fact that at low frequencies the tool causes a uniform shift in the phase velocities of the tube wave (Cheng and Toksöz, 1981). An equivalent result could be obtained by scaling the wavenumbers. The results of some numerical experiments indicated that the errors introduced by this scaling are very small. The main advantages of this method are that it is simple and that the original mathematical model and dispersion equation can be used.

To determine the best scaling, a two-step process was used. First, wavenumbers were calculated by processing seismograms from a formation which had low permeability (i.e., 26 to 33 mD) and low gamma ray emissions (i.e., 75 to 95 GAPI units). Low permeability (i.e., less than about 100 mD) is important because permeability can affect the velocity dispersion of the tube wave (Cheng et al., 1987). The low emissions indicate that few clay minerals are present, and because these minerals are a major cause of transverse isotropy their small concentration suggests that the formation is mostly isotropic. Second, c_{66} was estimated with different scaling factors for the wavenumbers until c_{66} was fairly close to c_{44}; this match is necessary because c_{66} equals c_{44} in isotropic formations. The best scaling factor was 0.94.

The field logs were used to find a zone where accurate values of c_{66} could be estimated. The cores indicate that rock in this zone is mostly siltstone. The permeability ranges from 0.1 to 110 mD (Figure 20) which is low enough that the estimate for c_{66} will not be affected. The borehole wall is smooth (Figure 21), which reduces the scattering of the waves and makes the processing results more accurate. The difference between the drill bit size and the measured radius is small (i.e., about 0.005 m) indicating that shale hydration is not a severe problem. The gamma ray emission is high (Figure 22) indicating that the formation has many clay minerals and might be transversely isotropic. The vertical S wave velocity is high (Figure 23) indicating that (if the formation is transversely isotropic) the tube wave will be more sensitive to c_{66} than the other elastic moduli. The density corrections are small (Figure 24) indicating that the density measurements are reliable. The acoustic logging data show no reflections (Figure 25) indicating that the elastic properties of contiguous beds are similar and that large fractures are not present.

At each depth, the wavenumbers for the tube wave were calculated by combining the data from both sources. That is, the wavenumbers were calculated from 2 data

sets, each of which contained 12 seismograms from the 12 receivers. A few inaccurate wavenumber estimates were obtained, and these were deleted before the inversion was performed. The model parameters (i.e., c_{11}, c_{13}, c_{33}, c_{44}, a starting value for c_{66}, σ_M, ρ_2, and R) were determined from the logs (Figures 21, 23, and 24) and cross plots (Figures 2, 12 and 13). c_{66} was determined at twenty successive depths using $p = 1.8$ (Figure 26). These estimates are actually an average of the value of c_{66}. That is, the data from all receivers at one depth are combined to obtain one estimate even though this modulus probably changes over the length of the receiver array. The estimates for c_{66} should change smoothly because the logging tool only moves a fraction of the length of the receiver array between successive depths. The scatter in the estimates is caused by slightly inaccurate wavenumber estimates. The scatter has been removed with smoothing, and the estimated values appear to be within about 15% of the smoothed values. The smoothed values for c_{66} (and even the original estimates) are significantly higher than c_{44} which is typical of transversely isotropic rocks (see Thomsen, 1986). Another way of comparing these moduli is based upon the percentage of S wave anisotropy, which is defined as

$$\frac{v_{SH} - v_{SV}}{v_{SV}} \times 100\%$$

where v_{SH} and v_{SV} are the velocities of horizontally propagating S waves with horizontal and vertical polarizations, respectively. In this zone, the S wave anisotropy ranges from 19 to 24% (Figure 27) based upon the smoothed values for c_{66}.

CONCLUSIONS

Sensitivities, which are normalized partial derivatives, indicate how the wavenumbers for the tube wave are affected by the elastic moduli of the fluid and the formation. At low frequencies the wavenumbers for the tube wave in fast and slow formations are very sensitive to λ_1 and moderately sensitive to c_{66}. Therefore, an accurate value for λ_1 must be obtained before a value for c_{66} is estimated. The wavenumbers are insensitive to c_{11}, c_{13}, c_{33} at all frequencies, and are only moderately sensitive to c_{44} near 5 kHz. Consequently, the inversion for c_{66} will not be adversely affected if slightly inaccurate values for these moduli are picked. In very slow formations, the wavenumbers for the tube wave are as sensitive to the unknown moduli c_{11} and c_{13} as they are to c_{66}. Hence c_{66} cannot be estimated for very slow formations. A useful rule of thumb is that c_{66} should be estimated only when the vertical S wave velocity is greater than or nearly equal to the acoustic velocity of the fluid.

The inversion for c_{66} is based upon a cost function which combines information about the wavenumbers, the expected values for c_{66}, and the physical constraints on its value. The cost function is minimized using a robust method which prevents large residuals in the wavenumbers from adversely affecting the result. When the inversion

was applied to synthetic data from fast and slow formations, the estimates for c_{66} were within 5% of their correct values and were well resolved. The inversion was applied to field data from a formation which consists mostly of siltstone. All estimates for c_{66} were significantly higher than c_{44}, and the percentage of S wave anisotropy ranged from 19 to 24%.

ACKNOWLEDGEMENTS

This work was supported by the Full Waveform Acoustic Logging Consortium at M.I.T. K. J. Ellefsen was partially supported by the Phillips Petroleum Fellowship.

REFERENCES

Aki, K. and P. G. Richards, *Quantitative Seismology,* W. H. Freeman & Co., 1980.

Auld, B. A., *Acoustic Fields and Waves in Solids,* vol. 1, John Wiley & Sons, Inc., 1973.

Bard, Y., *Nonlinear Parameter Estimation,* Academic Press Inc., 1974.

Chan, A. K. and L. Tsang, Propagation of acoustic waves in a fluid-filled borehole surrounded by a concentrically layered transversely isotropic formation, *J. Acoust. Soc. Am., 74,* 1605–1616, 1983.

Cheng, C. H. and M. N. Toksöz, Elastic wave propagation in a fluid-filled borehole and synthetic acoustic logs, *Geophysics, 46,* 1042–1053, 1981.

Cheng, C. H., J. Zhang, and D. R. Burns, Effects of in-situ permeability on the propagation of Stoneley (tube) waves in a borehole, *Geophysics, 52,* 1279–1289, 1987.

Ellefsen, K. J., C. H. Cheng, and D. P. Schmitt, Acoustic logging guided waves in transversely isotropic formations, in *Trans., Soc. Prof. Well Log Analysts, 29th Ann. Log. Symp.,* 1988, paper YY.

Ellefsen, K. J., C. H. Cheng, and K. M. Tubman, Estimating phase velocity and attentuation of guided waves in acoustic logging data, *Geophysics, 54,* 1054–1059, 1989.

McClellan, J. H., Two-dimensional spectrum analysis in sonic logging, *Acoustics, Speech, Signal Processing Magazine, 3,* 12–18, 1986.

Moré, J. J., The Levenberg-Marquardt algorithm: Implementation and theory, in *Lecture Notes in Mathematics, no. 630,* edited by G. A. Watson, pp. 105–116, Springer-Verlag, 1978.

Moré, J. J., B. S. Garbow, and K. E. Hillstrom, *Users Guide for Minpack-1,* Argonne National Laboratory, 1982.

Parks, T. W., J. H. McClellan, and C. F. Morris, Algorithms for full-waveform sonic logging, in *Proceedings of the Second Acoustics, Speech, and Signal Processing Workshop on Spectral Estimation,* pp. 186–191, Tampa, Florida, 1983.

Scales, J. A. and A. Gersztenkorn, Robust methods in inverse theory, *Inverse Problems, 4,* 1071–1091, 1988.

Tarantola, A., *Inverse Problem Theory,* Elsevier Science Publ. Co., Inc., 1987.

Thomsen, L., Weak elastic anisotropy, *Geophysics, 51,* 1954–1966, 1986.

White, J. E. and C. Tongtaow, Cylindrical waves in transversely isotropic media, *J. Acoust. Soc. Am., 70,* 1147–1155, 1981.

White, J. E., L. Martineau-Nicholetis, and C. Monash, Measured anisotropy in Pierre shale, *Geophys. Prosp., 31,* 709–729, 1983.

Winterstein, D. F., Anisotropy effects in *P*-wave and *SH*-wave stacking velocities contain information on lithology, *Geophysics, 51,* 661–672, 1986.

Quantity	Value	Value used for Inversion
c_{11}	3.126×10^{10} Pa	3.0×10^{10} Pa
c_{13}	0.345×10^{10} Pa	1.1×10^{10} Pa
c_{33}	2.249×10^{10} Pa	2.1×10^{10} Pa
c_{44}	0.649×10^{10} Pa	0.64×10^{10} Pa
c_{66}	0.882×10^{10} Pa	1.0×10^{10} Pa
ρ_2	2075. kg/m^3	2075. kg/m^3
λ_1	0.225×10^{10} Pa	0.225×10^{10} Pa
ρ_1	1000. kg/m^3	1000. kg/m^3
R	0.1016 m	0.1016 m

Table 1: Model with a formation which represents the Green River shale (Thomsen, 1986).

Quantity	Value	Value used for Inversion
c_{11}	3.395×10^{10} Pa	3.0×10^{10} Pa
c_{13}	1.058×10^{10} Pa	1.2×10^{10} Pa
c_{33}	2.248×10^{10} Pa	2.2×10^{10} Pa
c_{44}	0.537×10^{10} Pa	0.51×10^{10} Pa
c_{66}	1.053×10^{10} Pa	0.70×10^{10} Pa
ρ_2	2420. kg/m^3	2420. kg/m^3
λ_1	0.225×10^{10} Pa	0.225×10^{10} Pa
ρ_1	1000. kg/m^3	1000. kg/m^3
R	0.1016 m	0.1016 m

Table 2: Model with a slow formation which represents shale (5000) (Thomsen, 1986).

Quantity	Value
c_{11}	1.387×10^{10} Pa
c_{13}	0.803×10^{10} Pa
c_{33}	0.998×10^{10} Pa
c_{44}	0.177×10^{10} Pa
c_{66}	0.283×10^{10} Pa
ρ_2	2250. kg/m^3
λ_1	0.225×10^{10} Pa
ρ_1	1000. kg/m^3
R	0.1016 m

Table 3: Model with a very slow formation which represents the Pierre shale (Thomsen, 1986).

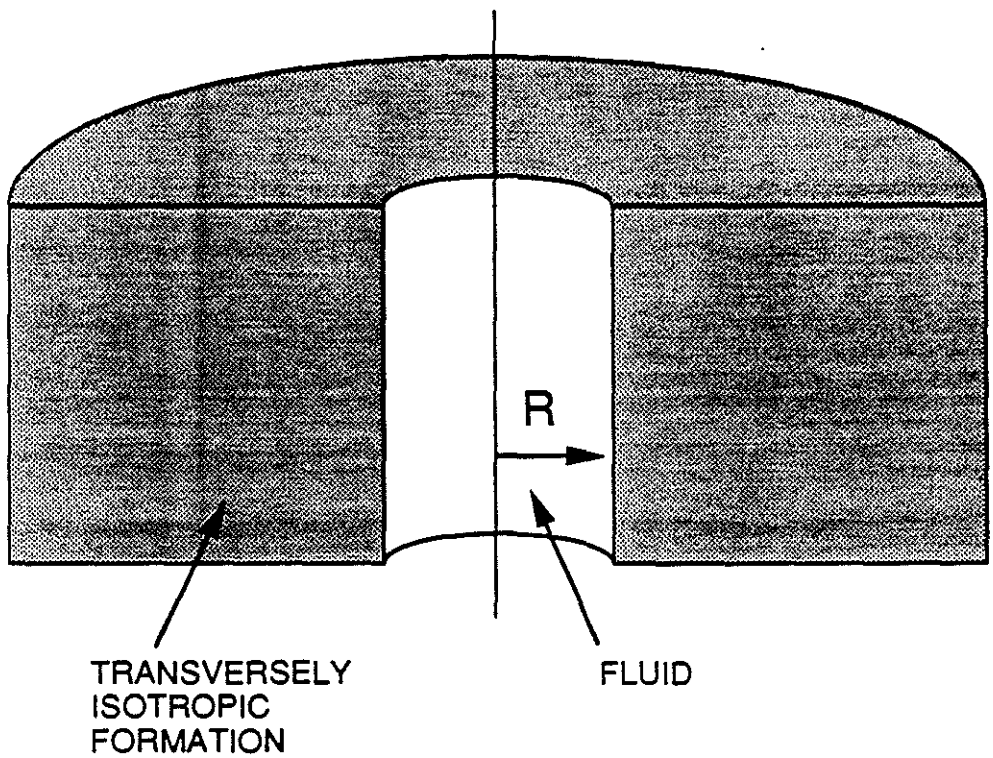

Figure 1: Mathematical model used for the inversion.

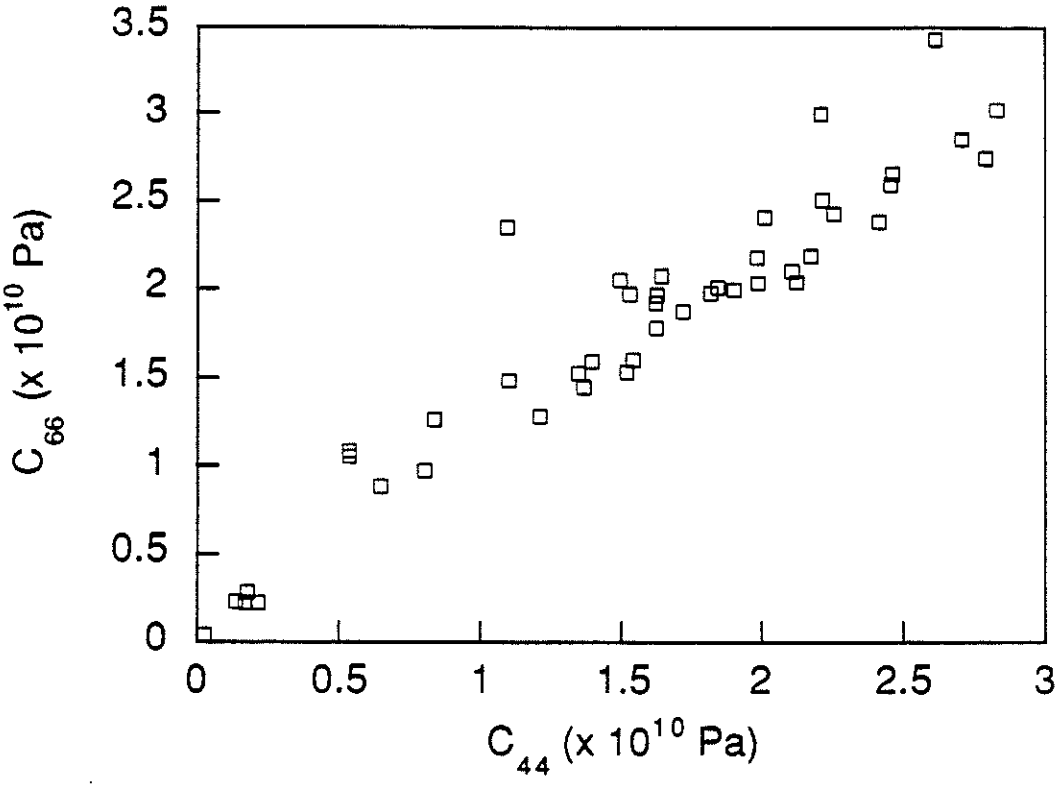

Figure 2: Cross-plot used to determine an initial value and standard deviation for c_{66}. The data are from the list of elastic moduli of transversely isotropic rocks compiled by Thomsen (1986).

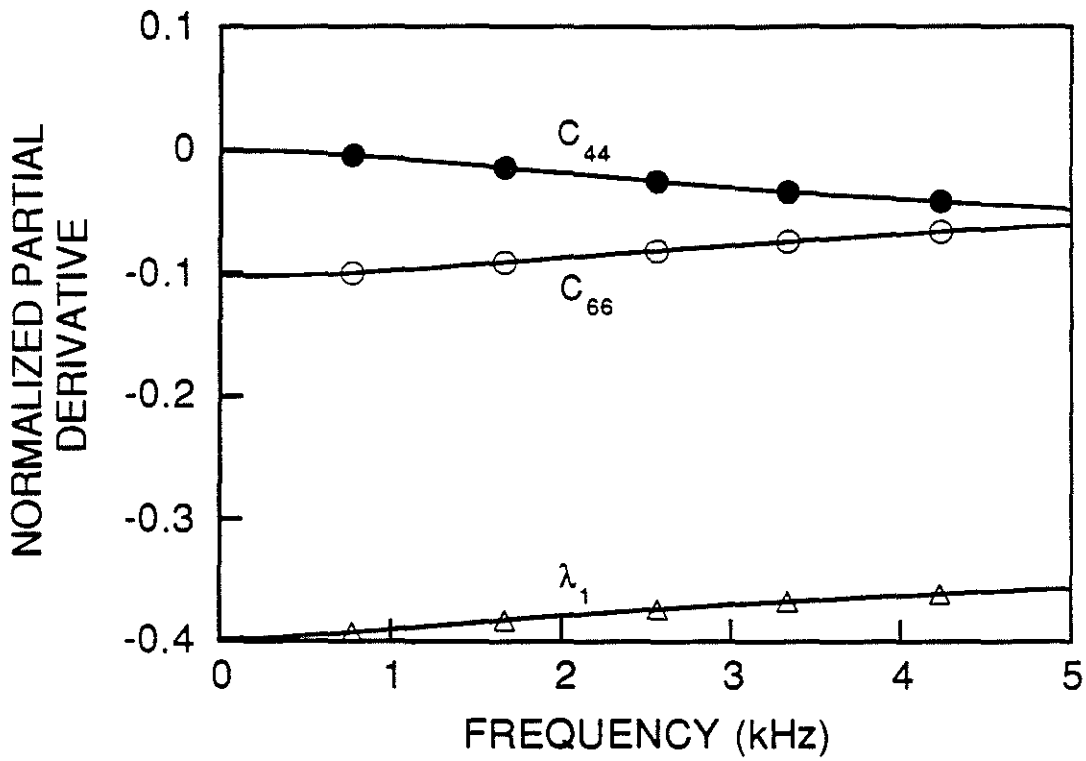

Figure 3: Sensitivities for the tube wave in the model with the fast formation (Table 1). See also Figure 4.

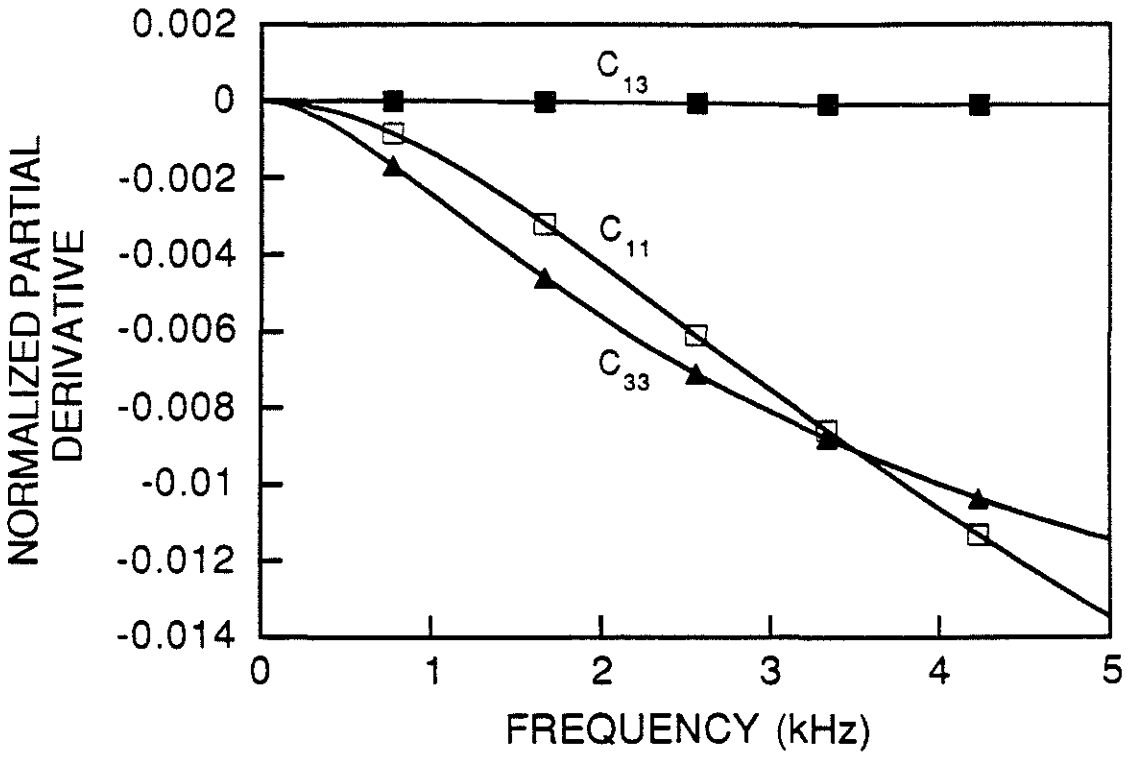

Figure 4: Sensitivities for the tube wave in the model with the fast formation (Table 1). See also Figure 3.

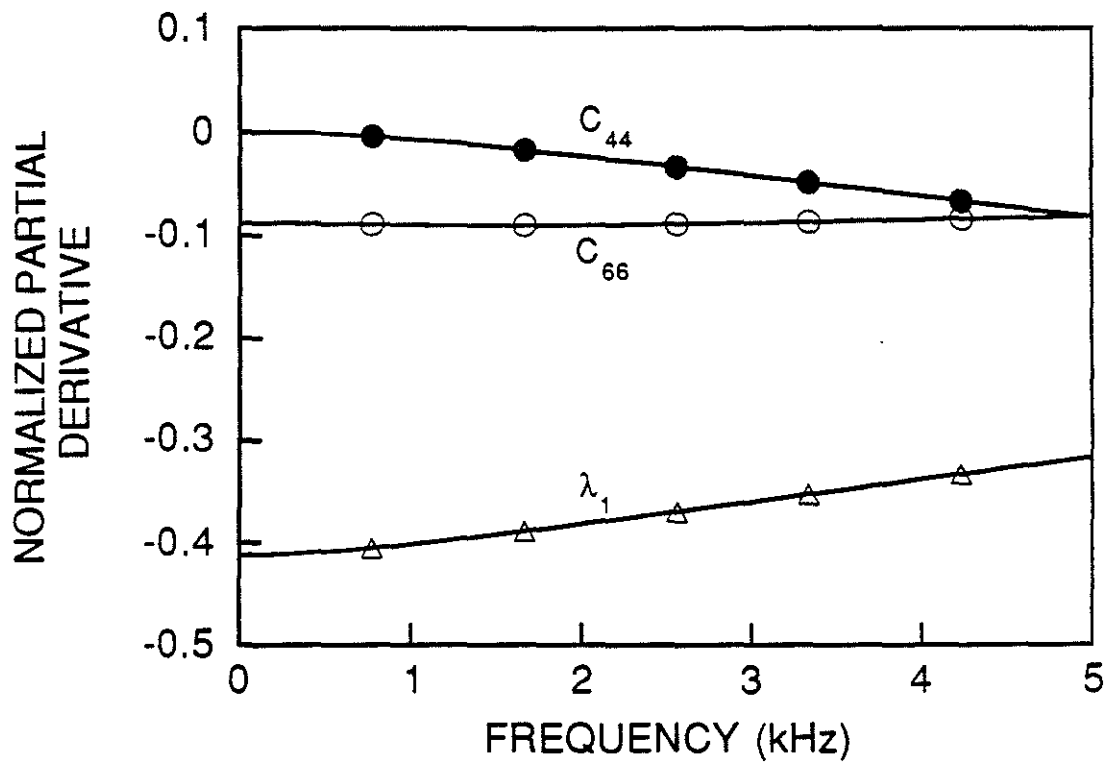

Figure 5: Sensitivities for the tube wave in the model with the slow formation (Table 2). See also Figure 6.

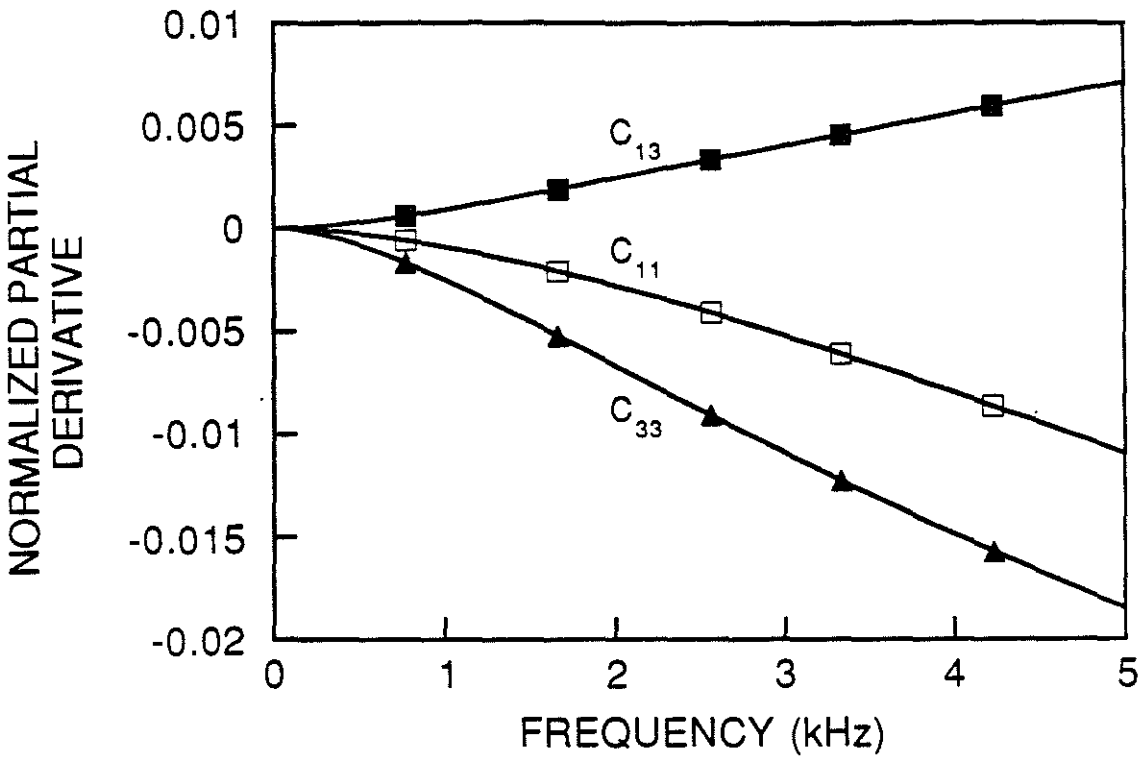

Figure 6: Sensitivities for the tube wave in the model with the slow formation (Table 2). See also Figure 5.

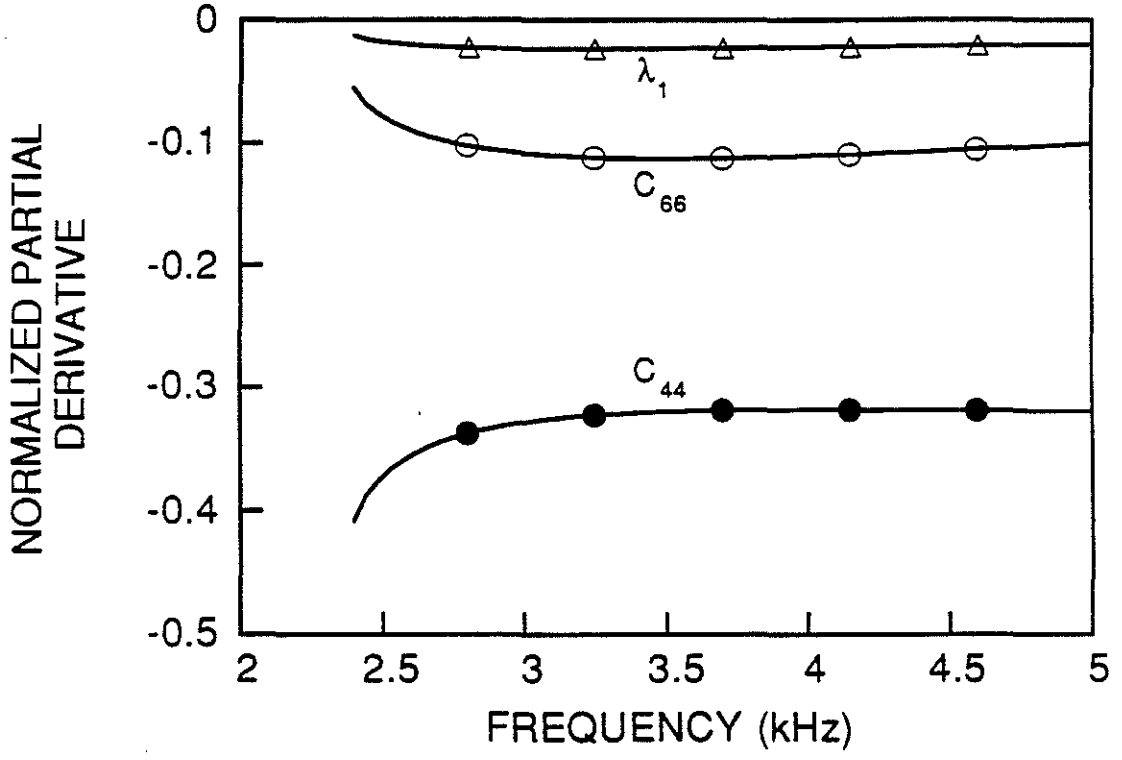

Figure 7: Sensitivities for the tube wave in the model with the very slow formation (Table 3). See also Figure 8.

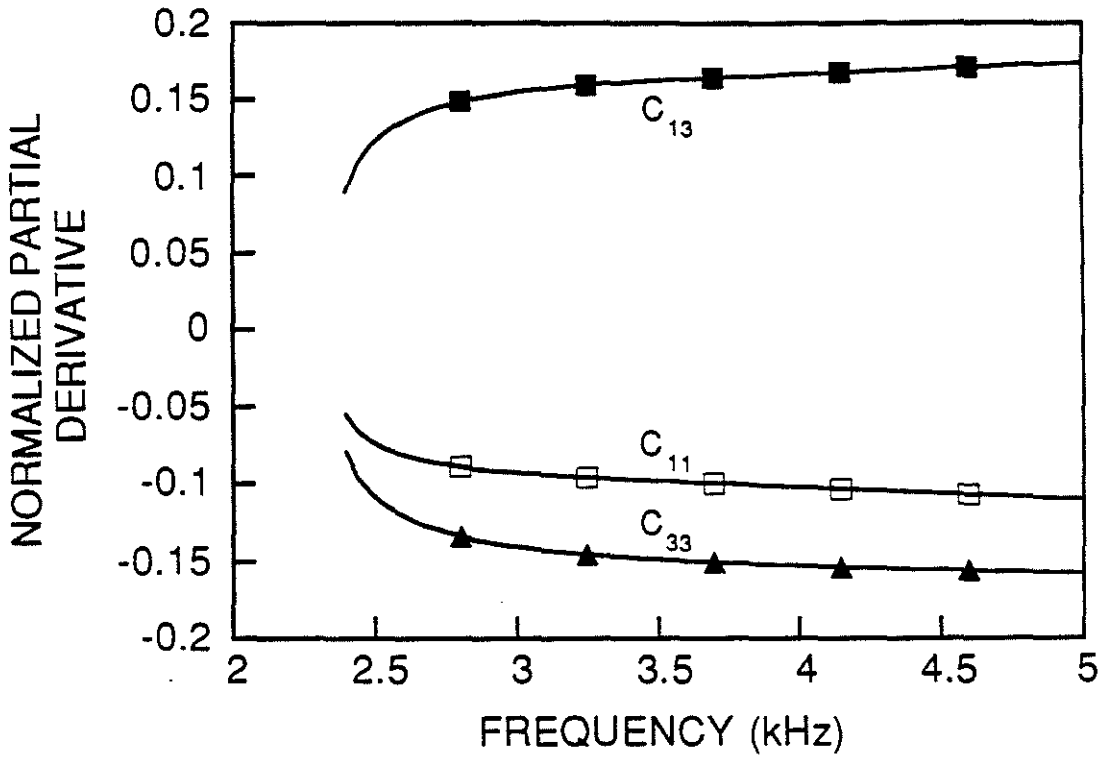

Figure 8: Sensitivities for the tube wave in the model with the very slow formation (Table 3). See also Figure 7.

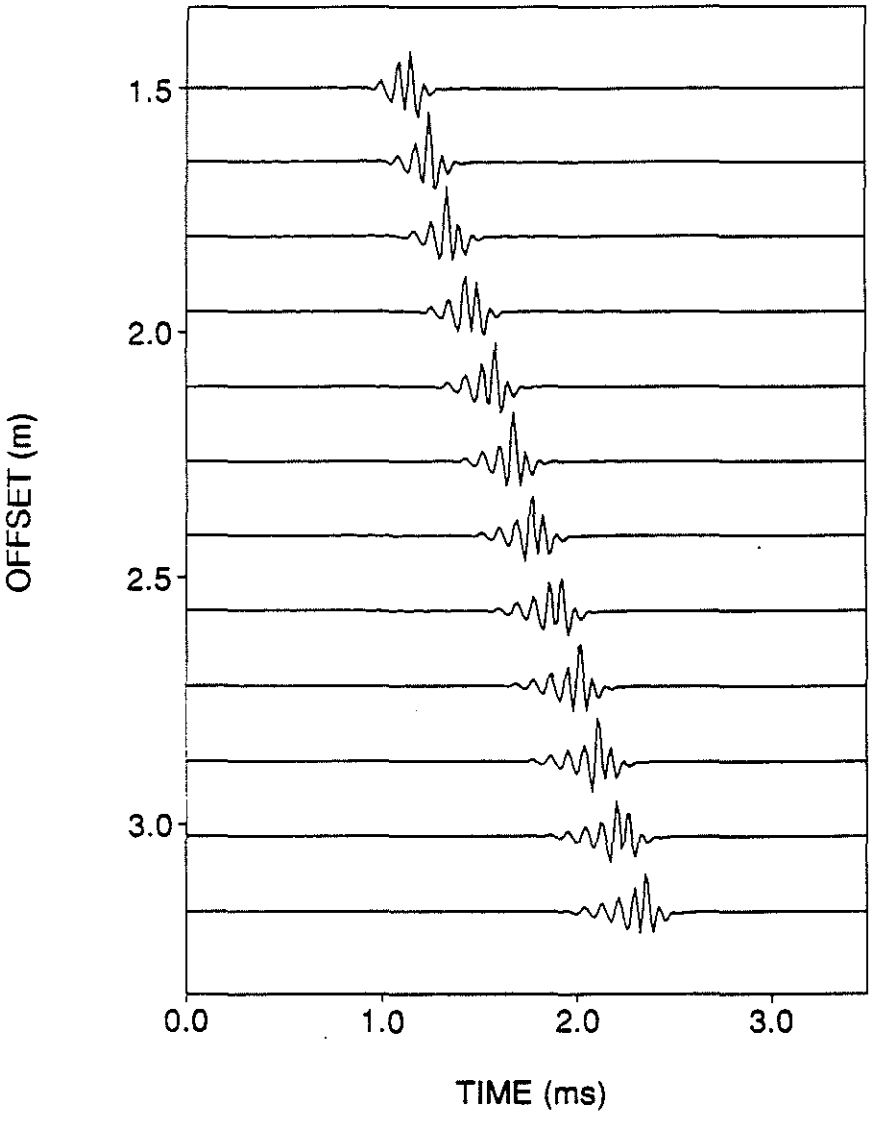

Figure 9: Synthetic seismograms for the model with the fast formation (Table 1).

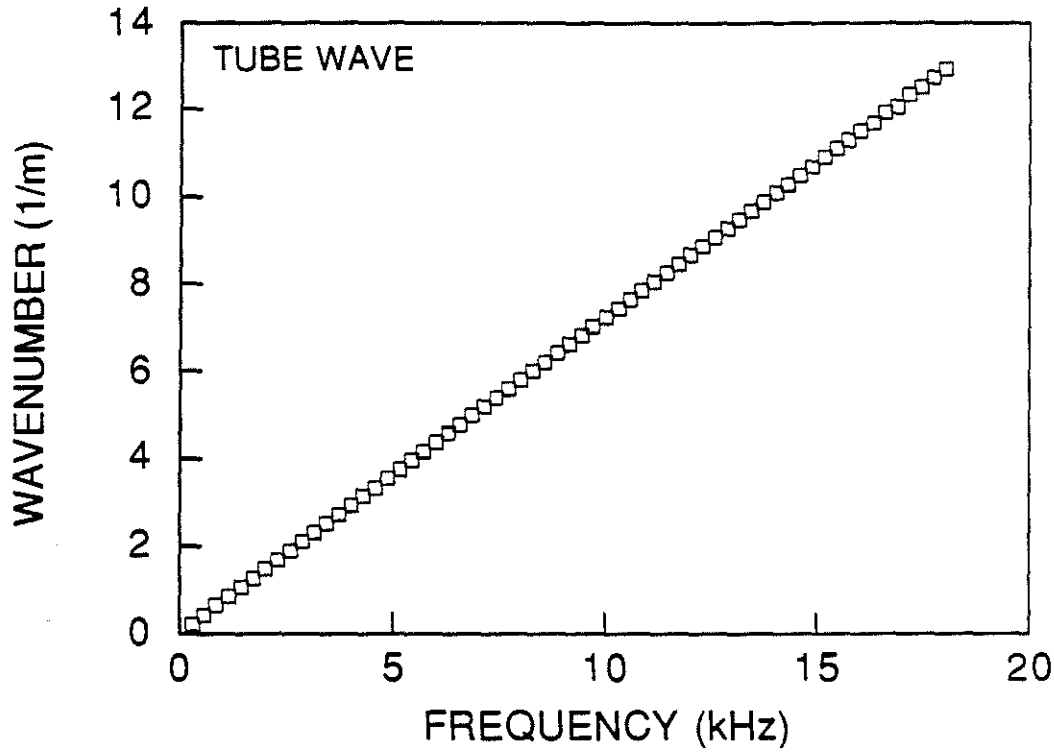

Figure 10: Wavenumber estimates for the tube wave obtained by processing the synthetic seismograms for the fast formation (Figure 9).

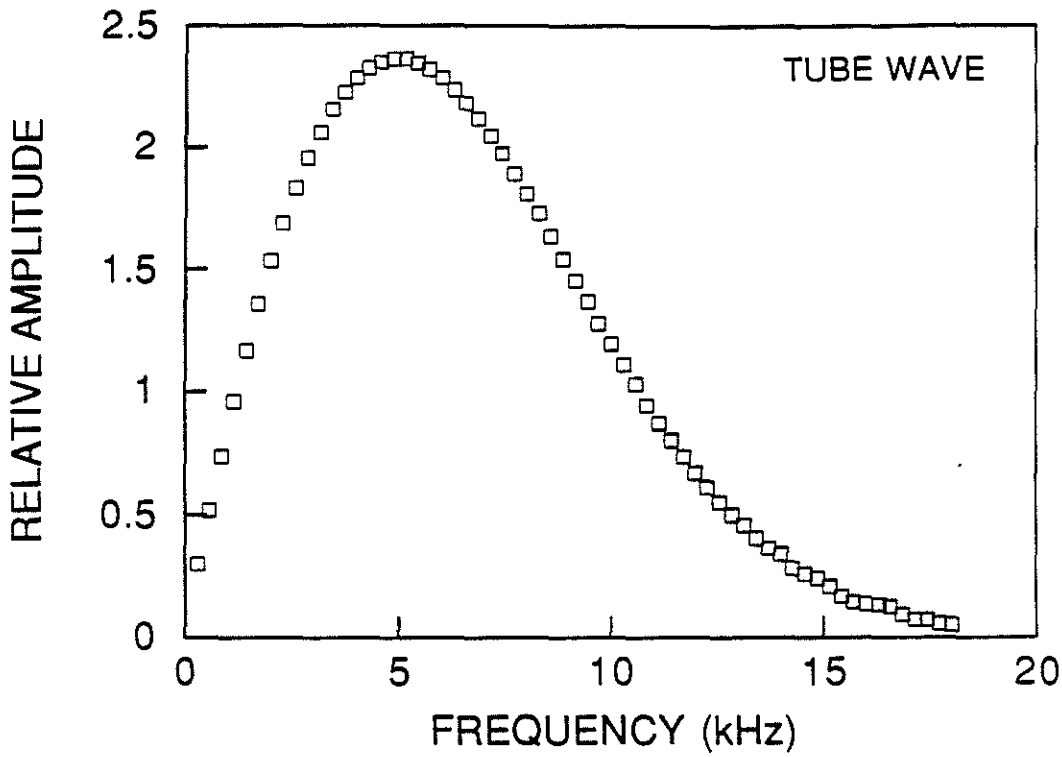

Figure 11: Amplitude estimates for the tube wave obtained by processing the synthetic seismograms for the fast formation (Figure 9).

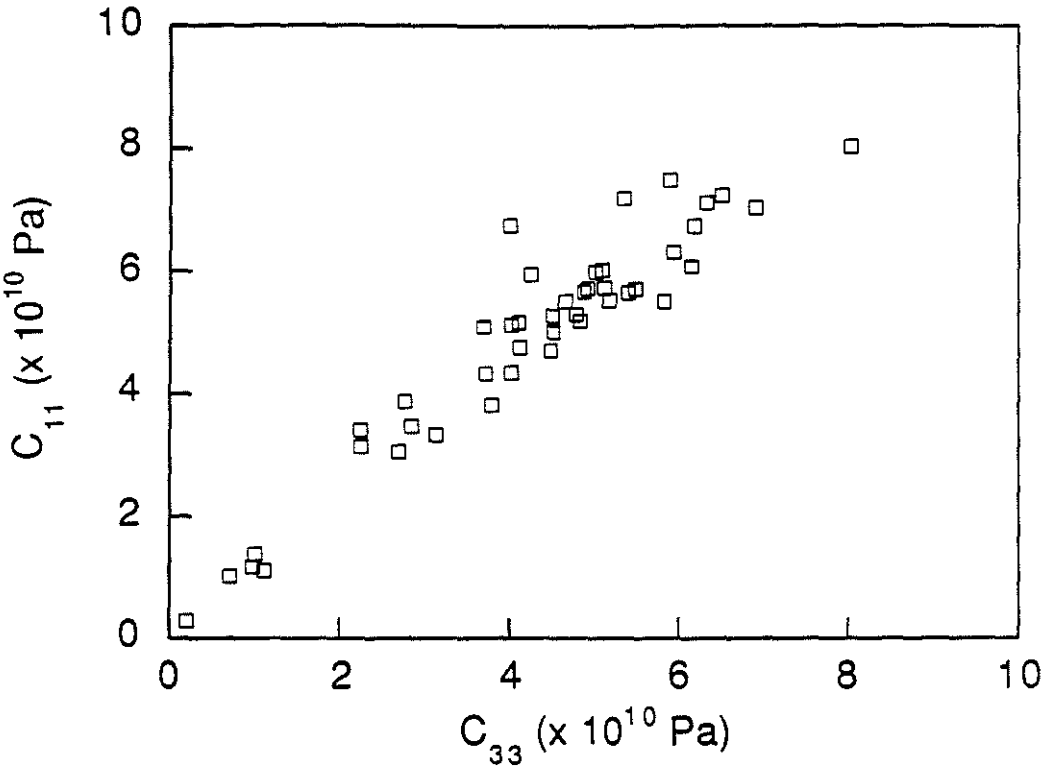

Figure 12: Cross-plot used to determine a reasonable value for c_{11}. The data are from the list of elastic moduli of transversely isotropic rocks compiled by Thomsen (1986).

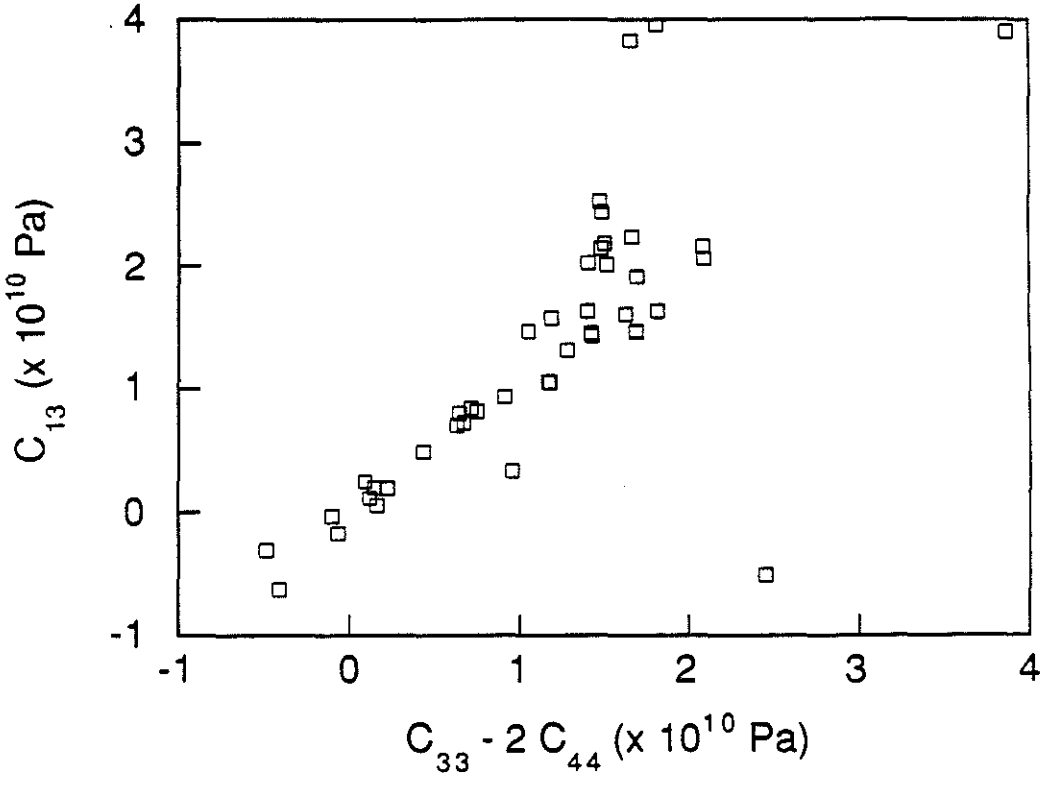

Figure 13: Cross-plot used to determine a reasonable value for c_{13}. The data are from the list of elastic moduli of transversely isotropic rocks compiled by Thomsen (1986).

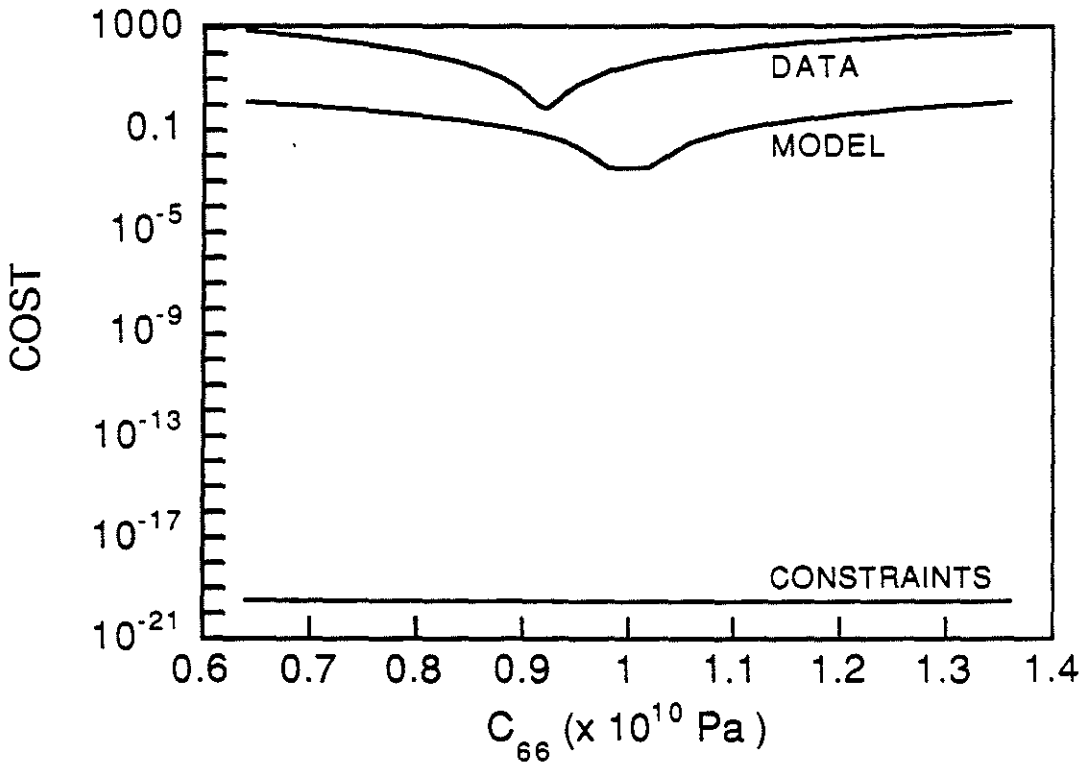

Figure 14: Terms in the cost function used to estimate c_{66} in the fast formation.

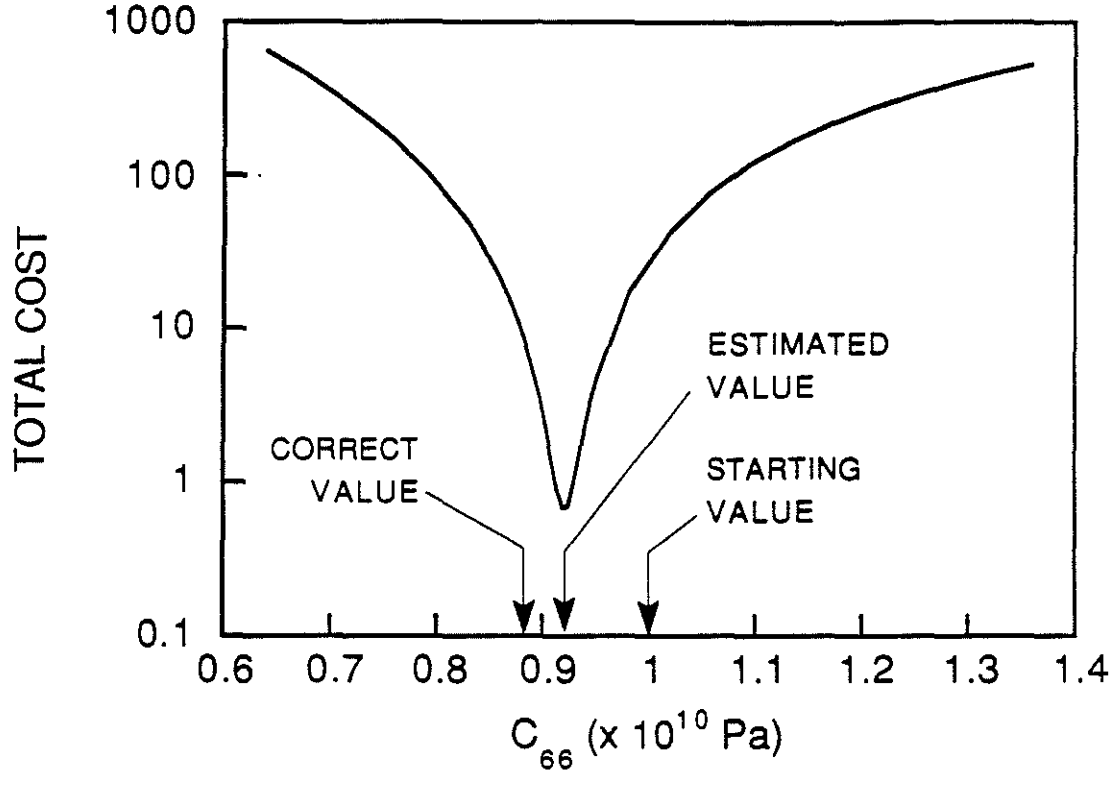

Figure 15: Cost surface for the estimation of c_{66} in the fast formation.

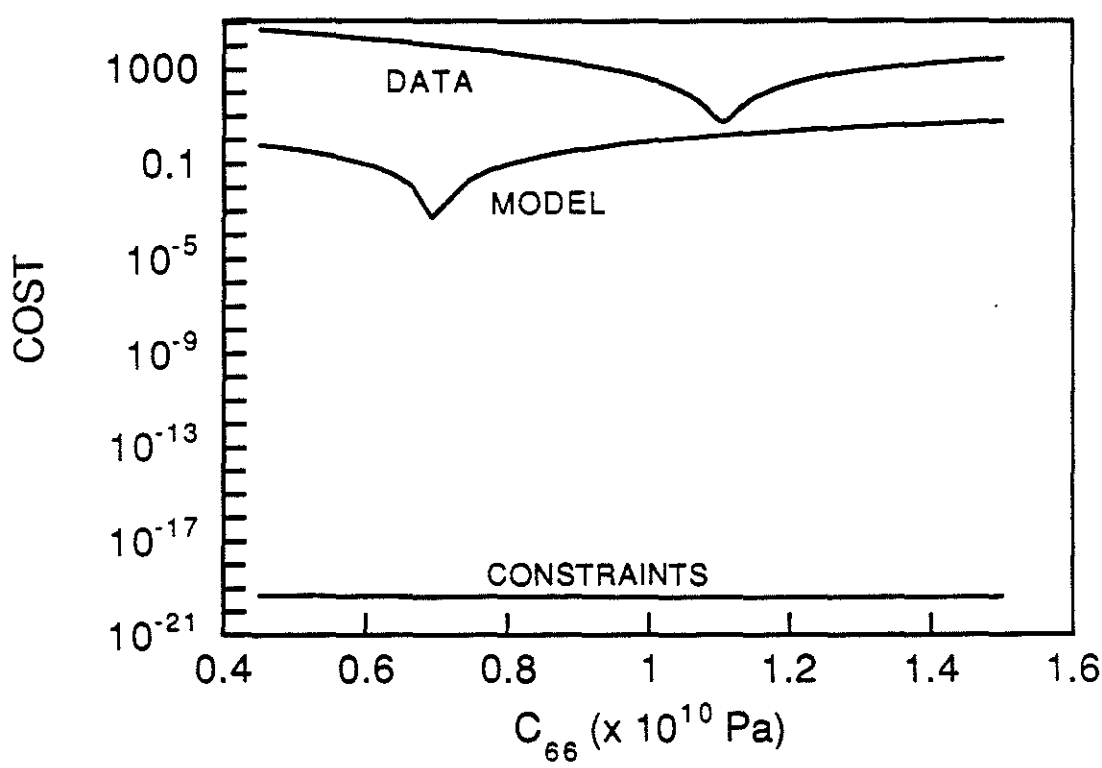

Figure 16: Terms in the cost function used to estimate c_{66} in the slow formation.

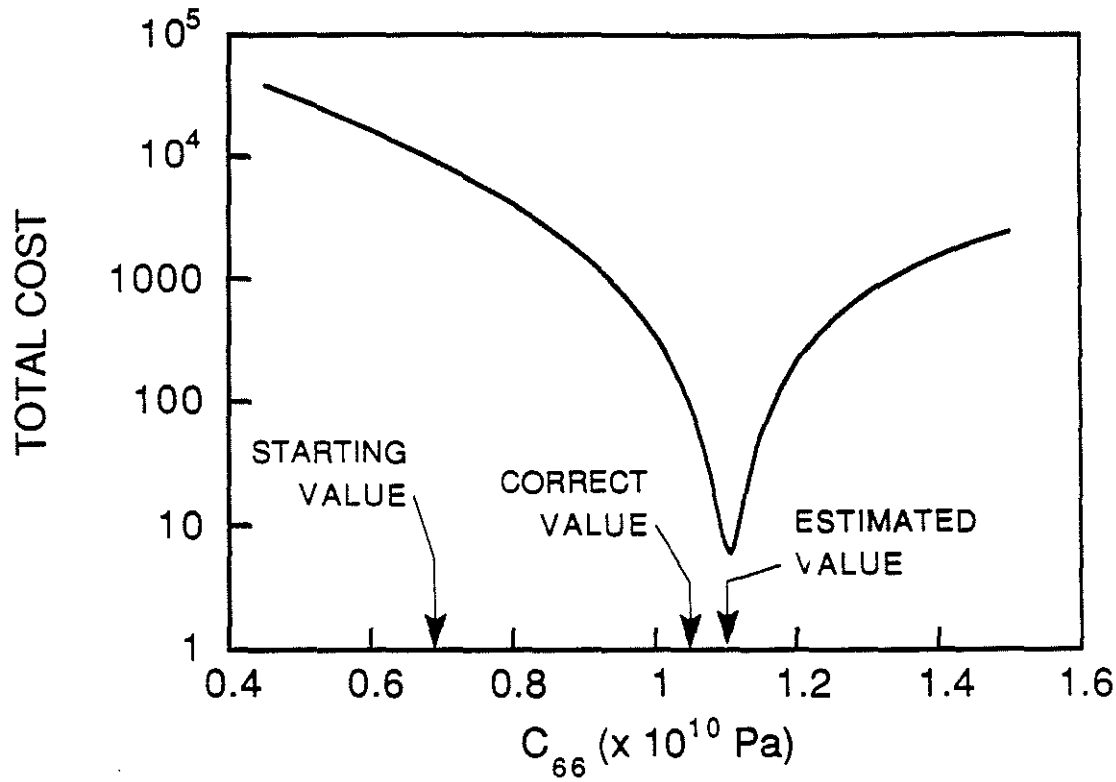

Figure 17: Cost surface for the estimation of c_{66} in the slow formation.

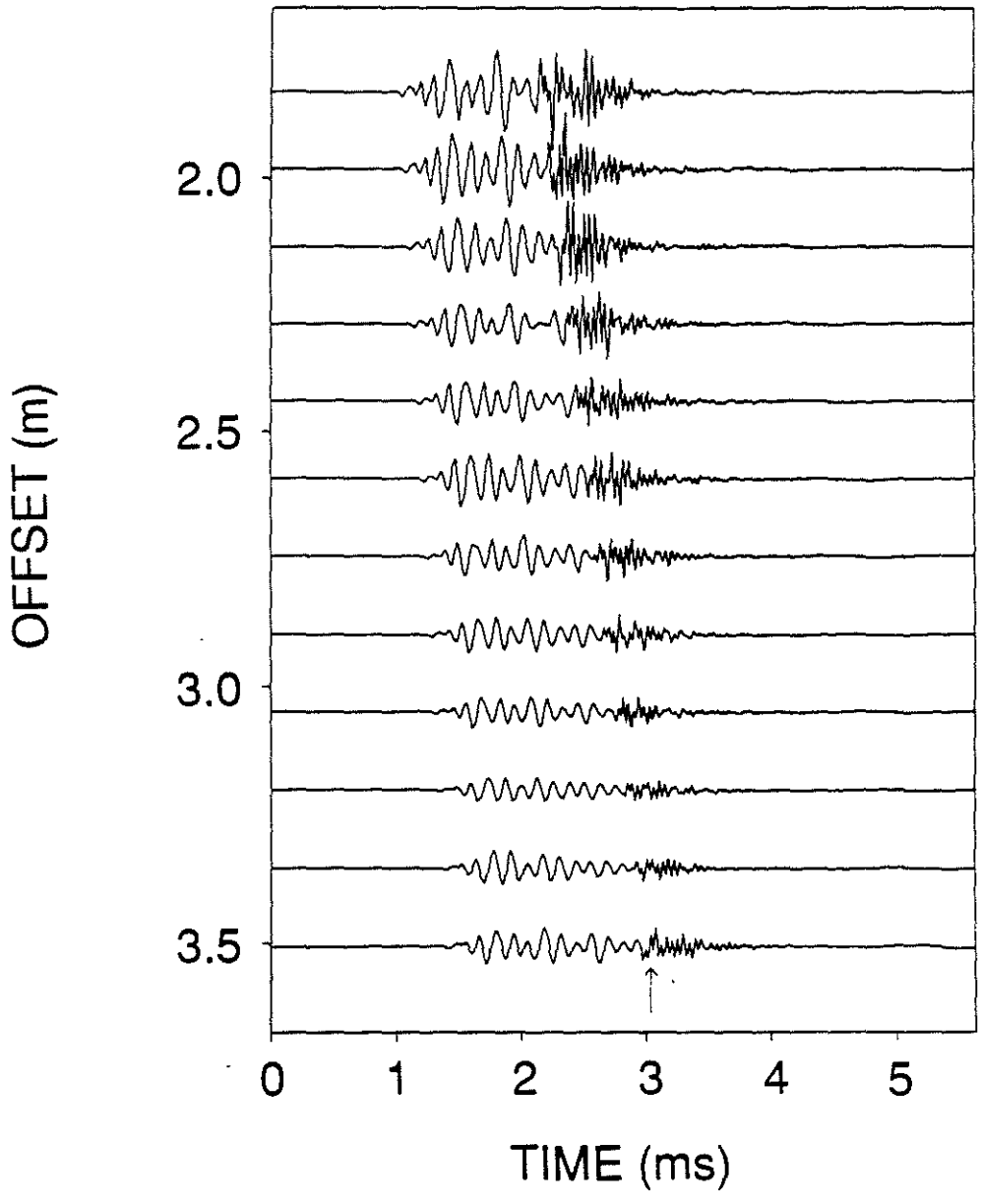

Figure 18: Seismograms used to estimate the phase velocity of the high frequency portion of the first leaky P mode, which is indicated by the arrow.

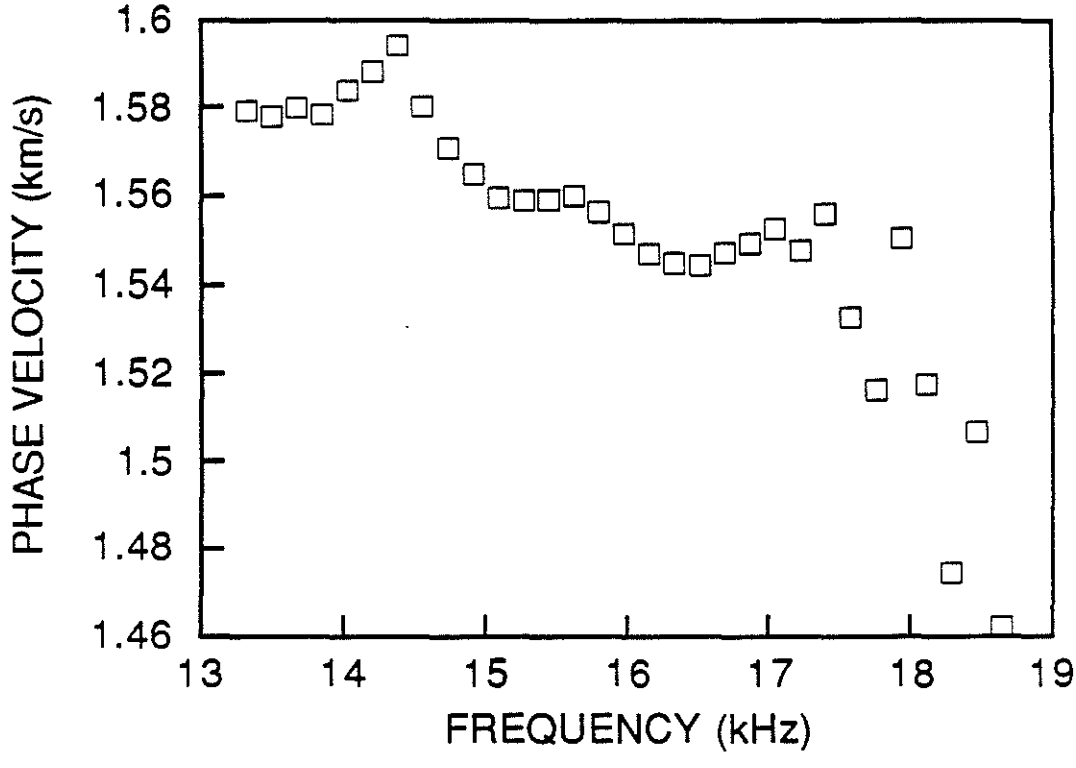

Figure 19: Phase velocity estimates for the high frequency portion of the first leaky P wave shown in Figure 18.

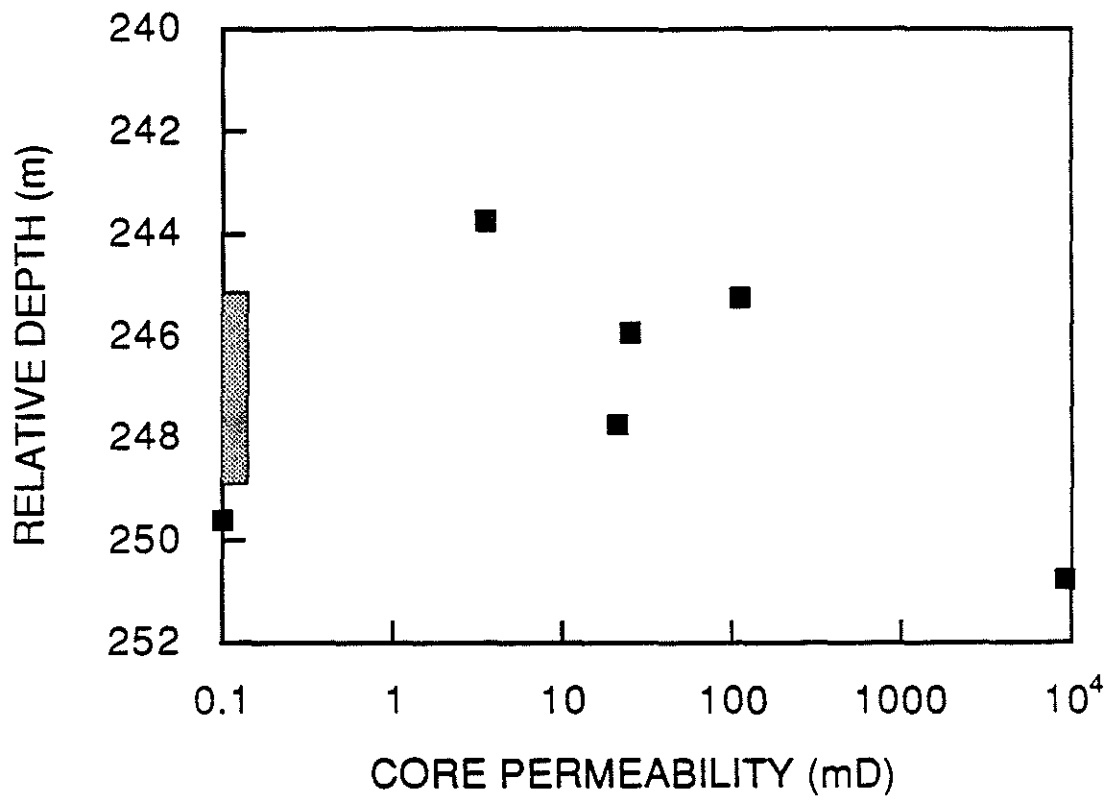

Figure 20: Permeability log. The shaded rectangle indicates the zone where c_{66} is estimated.

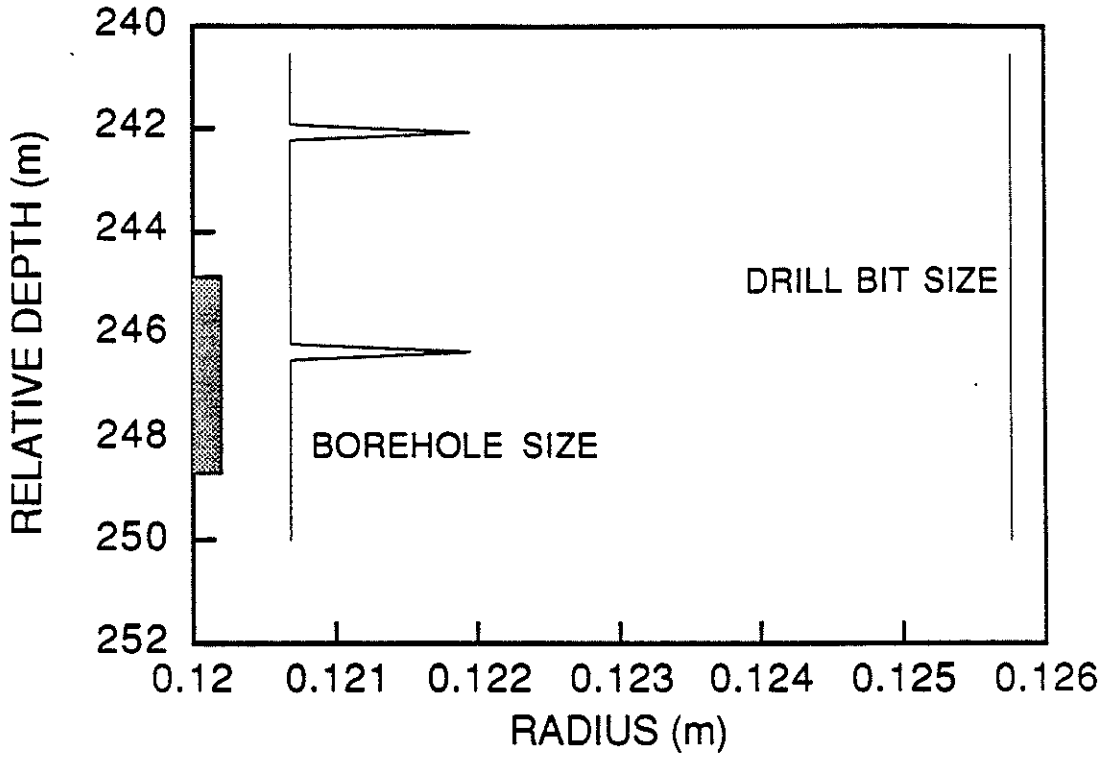

Figure 21: Caliper log. The shaded rectangle indicates the zone where c_{66} is estimated.

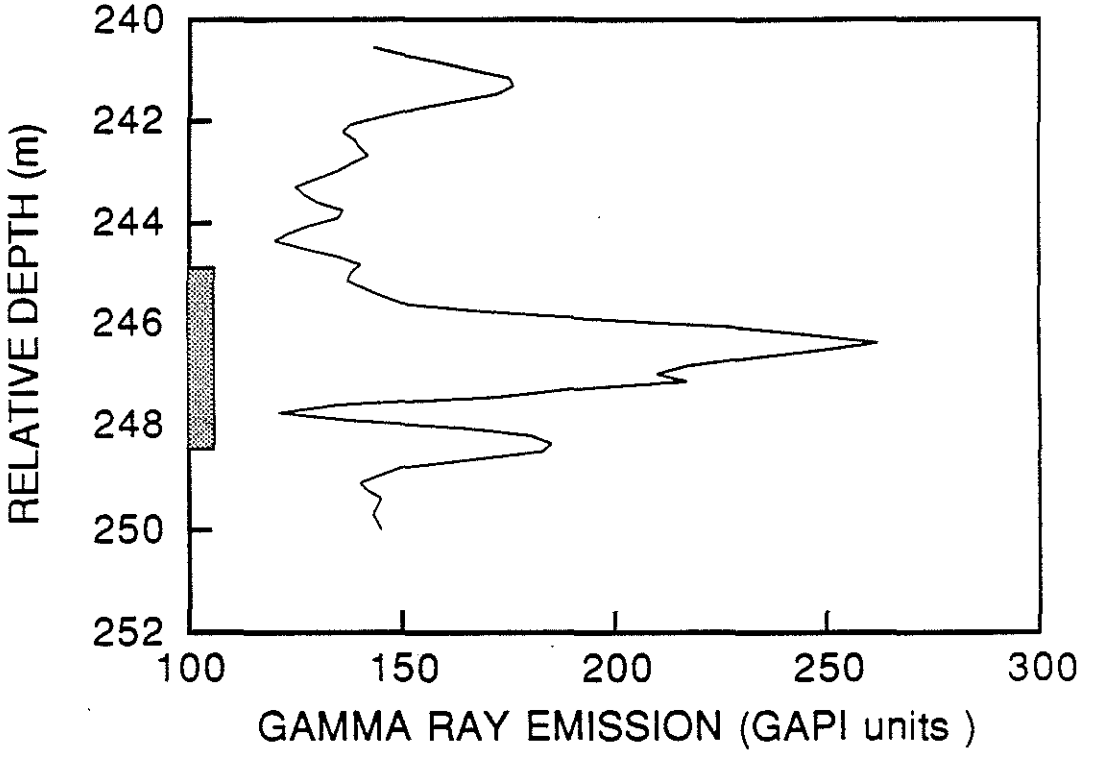

Figure 22: Gamma ray log. The shaded rectangle indicates the zone where c_{66} is estimated.

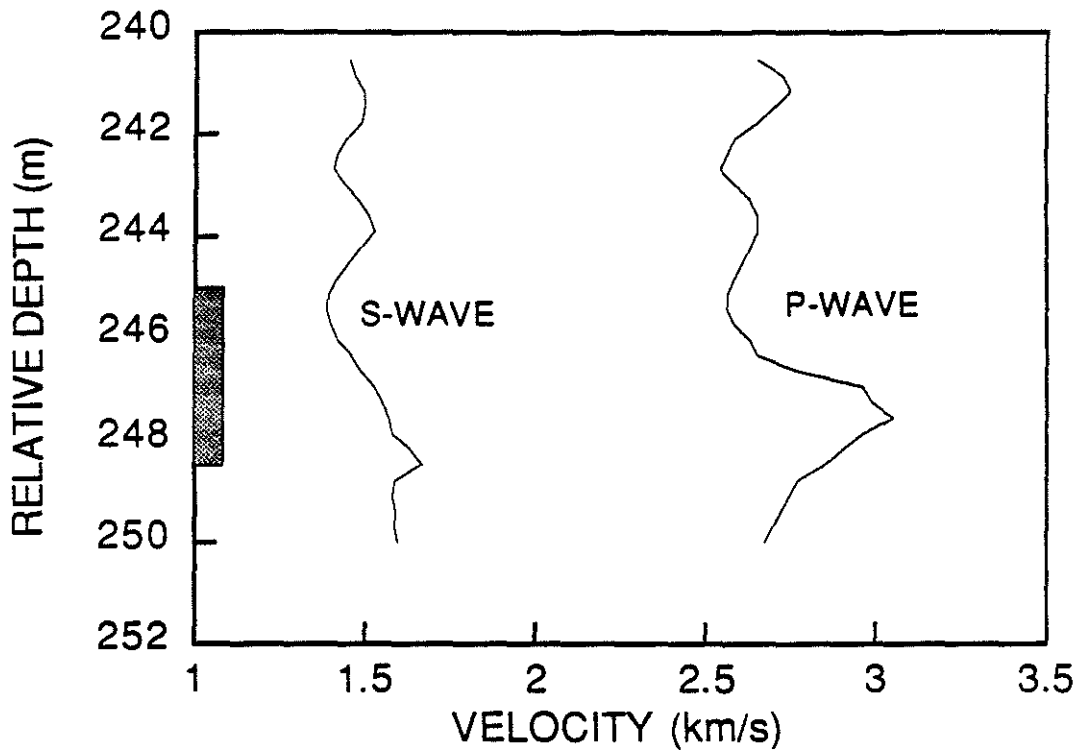

Figure 23: Velocity log. The shaded rectangle indicates the zone where c_{66} is estimated.

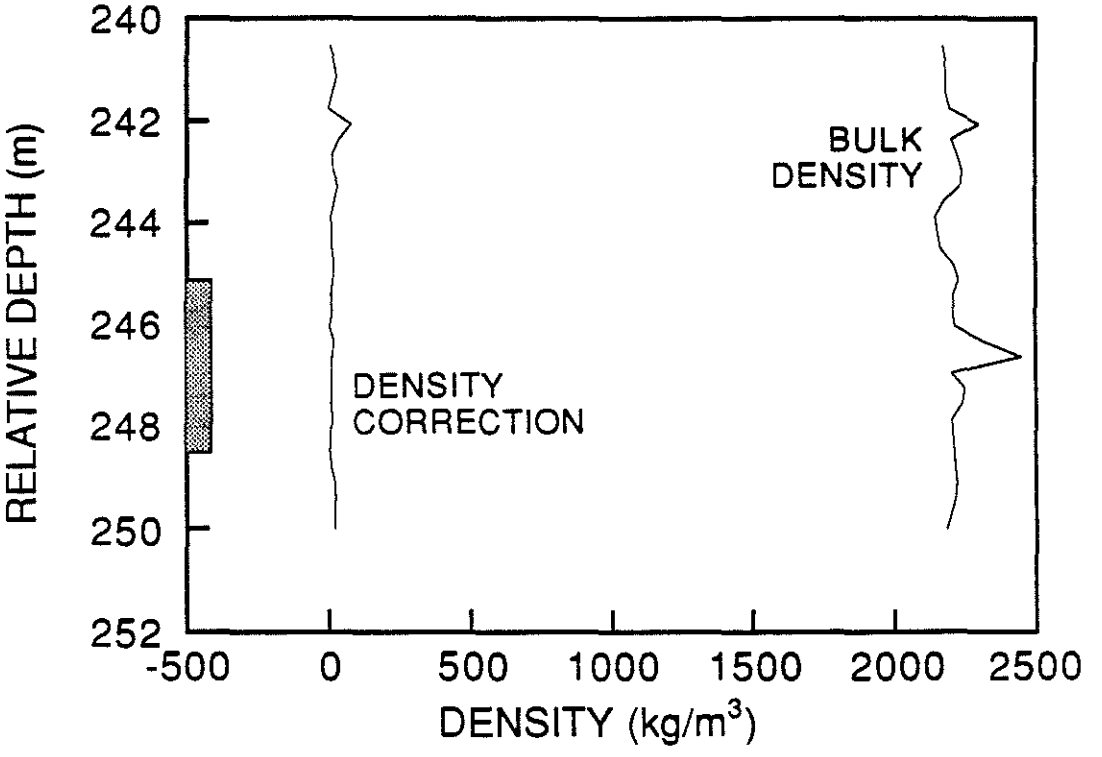

Figure 24: Density log. The shaded rectangle indicates the zone where c_{66} is estimated.

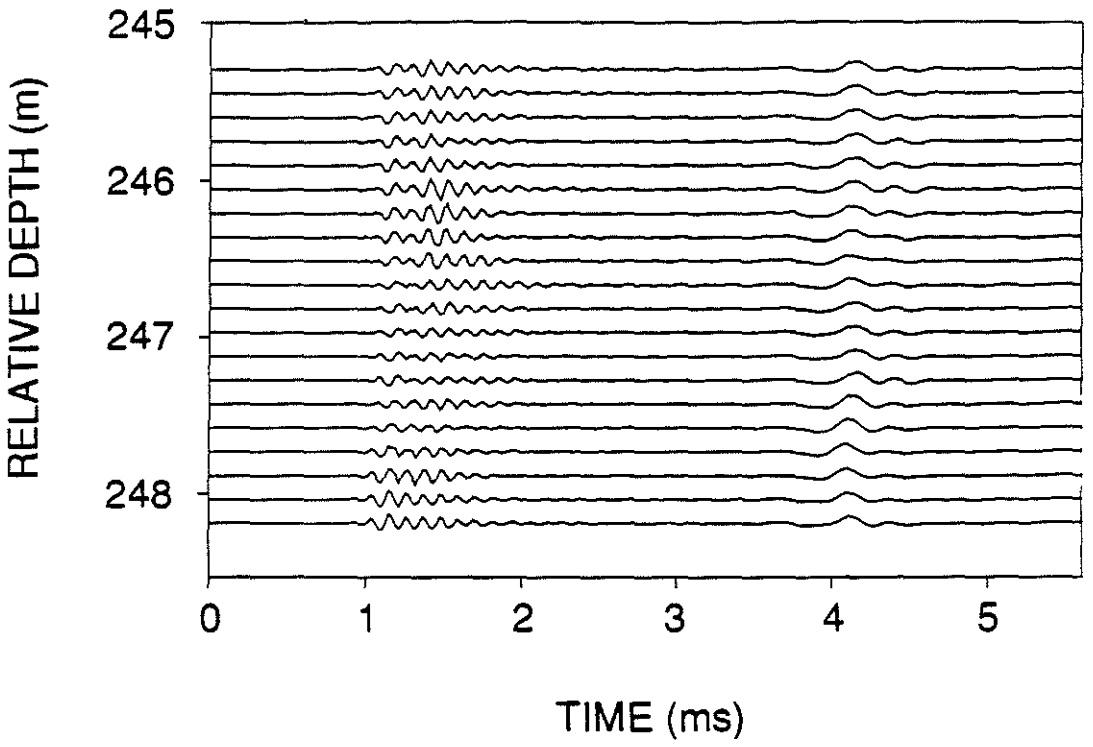

Figure 25: Seismograms recorded by the last receiver in the zone where c_{66} was estimated.

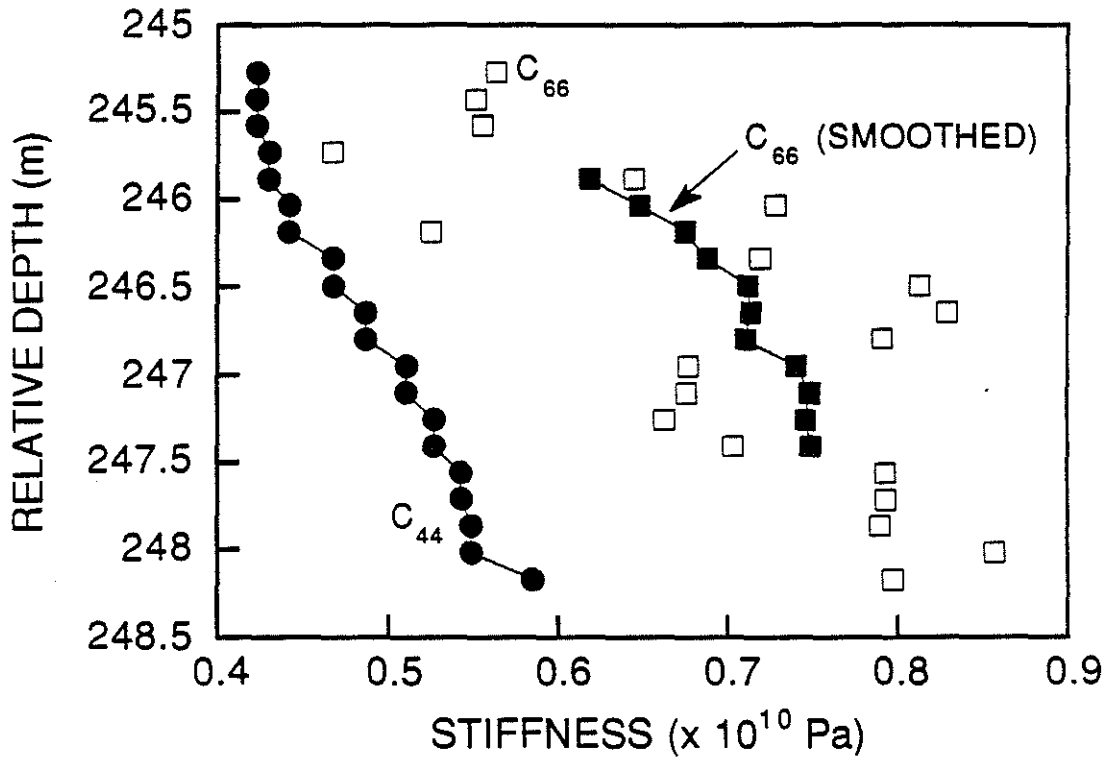

Figure 26: Estimates of c_{66} made from the tube wave, smoothed values for these estimates, and the values for c_{44} measured with the shear wave log.

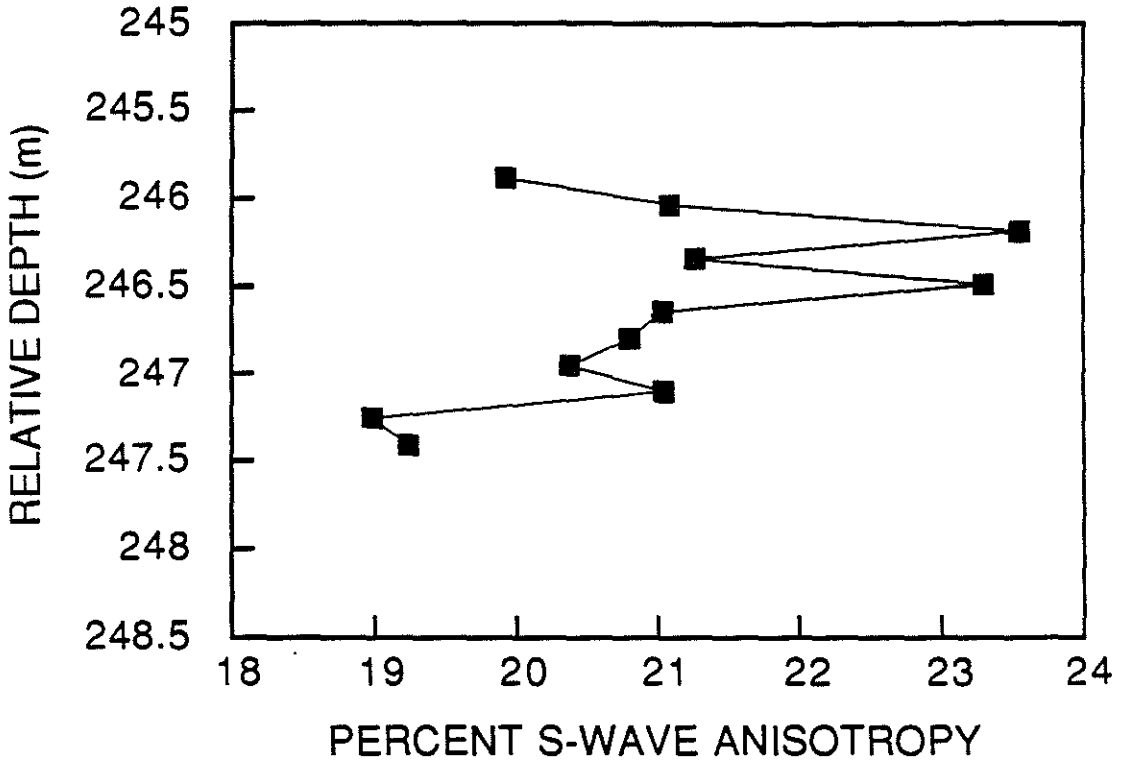

Figure 27: Percentage of S wave anisotropy calculated with the smoothed estimates of c_{66}.